Anisotropic Nucleation Growth of Actin Bundle: A Model for Determining the Well-Defined Thickness of Bundles†

Hyuck Joon Kwon,‡ Yoshimi Tanaka,§ Akira Kakugo,‡ Kazuhiro Shikinaka,‡ Hidemitsu Furukawa,‡ Yoshihito Osada,‡ and Jian Ping Gong*,‡,||

Department of Biological Science, Graduate School of Science, Hokkaido University, Sapporo 060-0810, Japan, Creative Research Initiative, Sapporo 011-0021, Japan, and SORST, JST, Sapporo 060-0810, Japan

Received April 14, 2006; Revised Manuscript Received July 6, 2006

ABSTRACT: Biopolymers such as DNA, F-actins, and microtubules, which are highly charged, rodlike polyelectrolytes, are assembled into architectures with defined morphology and size by electrostatic interaction with multivalent cations (or polycations) in vivo and in vitro. The physical origin to determine their morphology and size is not clearly understood yet. Our results show that the actin bundle formation consists of two stages: the thickness of actin bundles is determined nearly at the initial stage, while the length of actin bundles is determined later on. It is also found that the thickness of actin bundles decreases with the increase of polycation-mediated attraction between F-actins. From these results, we propose the anisotropic nucleation-growth mechanism, in which the thickness of actin bundles is determined by critical nucleus size, whereas the length of actin bundles is determined by the concentration of free actins relative to nucleus concentration. Observing that polycations are concentrated in some sites of actin bundles, which are thought to be nucleation sites to initiate the formation of actin bundles, supports this model. This anisotropic nucleation-growth mechanism of actin bundles can be broadly applied to the self-assembly of rodlike polyelectrolytes.

Biopolymers such as filamentous actin (F-actin),[1] DNA, and microtubule are rigid rodlike polyelectrolytes (*1*−*3*). These biopolymers, carrying negative charges, self-assemble into well-defined bundles, toroids, and networks by electrostatic interaction with multivalent cations (or polycations) both in vivo and in vitro (*2*−*21*). For example, the structure and the dynamics of the actin bundles and network are rigorously regulated by interaction with a number of actin binding proteins in the cell (*22*, *23*). Some of the actin binding proteins, such as Ena/VASP, calponin, dystrophin, and MARCKS, induce the formation of actin architectures, binding to actins by electrostatic interaction (*2*, *5*−*9*). Another example is found in the gene compaction process of the living cell or viruses where cationic proteins and polyamines are used in their DNA packaging (*10*, *11*). These facts indicate that the electrostatic interaction plays a central role in the organization of biopolymers in the cell.

Researchers have studied the counterion-mediated condensation of biopolymers and suggested a considerable number of theories to explain the physical origin to determine the defined size of biopolymer assemblies. It has been suggested that the growth of polyelectrolyte bundles is limited by electrostatic repulsion of polyelectrolytes uncompensated by counterions (*12*) or the kinetic barrier in bundling between polyelectrolytes (*13*). However, it was shown that the repulsion of the uncompensated polyelectrolytes cannot limit the bundle growth (*14*). In addition, it was reported that the larger DNA toroids are formed in higher ionic strength (*15*−*17*), which cannot be explained by the kinetic barrier in bundling of polyelectrolytes. Moreover, most theories have been concentrated in the formation of toroidal bundles limited in DNA (*12*, *15*−*19*). Thus, it is needed to construct a more general model to explain how the well-defined size of the polyelectrolyte bundles is determined by systematically investigating the defined thickness of polyelectrolyte bundles.

Here, we use a model system consisting of F-actin and polylysine (later denoted as p-Lys) to investigate the physical origin of the well-defined thickness D and length L of the polyelectrolyte bundles. Our study shows that D growth is nearly completed in the initial stage of bundle growth, while dramatic L growth starts later on, after completion of D growth. Additionally, D decreases with the increase in the polycation-mediated attraction between F-actins but is hardly influenced by the actin concentration (C_A), while L increases with the increase of C_A. We propose the new anisotropic nucleation-growth model in which D is determined by the critical nucleus size D_0, while the length L is determined by free actin concentration relative to nucleus concentration.

This anisotropic growth of actin bundles originates from the rodlike polyelectrolyte nature of F-actins. Therefore, our

† This work was supported by grants from SORST, JST.

* To whom correspondence should be addressed. E-mail: gong@sci.hokudai.ac.jp. Phone/Fax: 81(11)706-2774.

‡ Hokkaido University.

§ Creative Research Initiative.

|| SORST, JST.

[1] Abbreviations: F-actin, filamentous actin; D, thickness of actin bundle; D_0, thickness of a critical nucleus; L, length of actin bundle; C_P, polylysine (p-Lys) concentration in monomer unit; C_S, salt (KCl) concentration; C_A, actin concentration in monomer (G-actin) unit; C_P^c, critical p-Lys concentration for bundle formation; TEM, transmission electron microscopy.

10.1021/bi060721w CCC: $33.50
Published on Web 08/04/2006

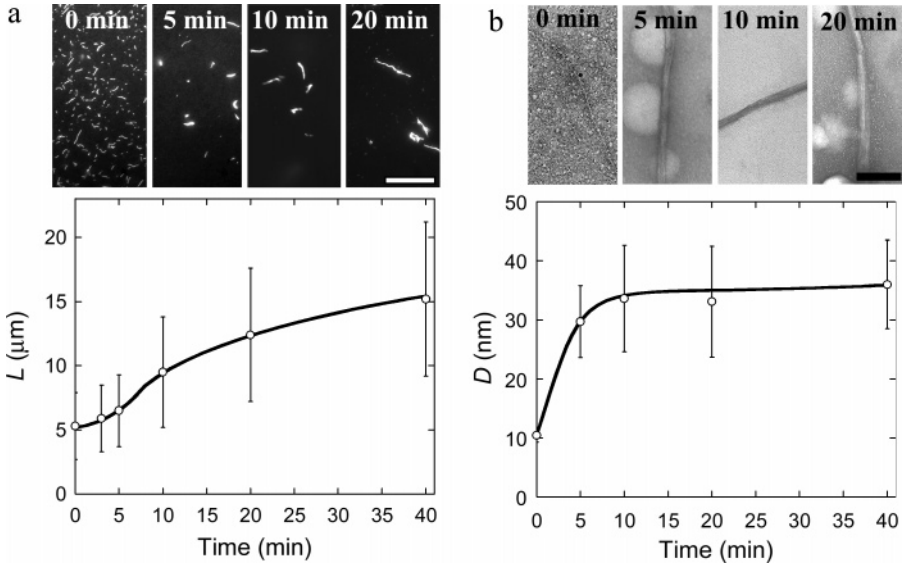

FIGURE 1: Kinetics of actin bundle formation by electrostatic interaction with p-Lys ($N = 26$). (a) Fluorescence images and time profile of bundle length L. (b) TEM images and time profile of bundle thickness D. $C_A = 4.6 \times 10^{-8}$ M, $C_P(N = 26) = 10^{-4}$ M, and $C_S = 0.1$ M. Scale bars represent 20 μm for fluorescence images and 200 nm for TEM images.

model not only provides insight into physical origins of how the growth of cellular actin bundles is determined but also can be broadly applied to the self-assembly of rodlike polyelectrolytes.

EXPERIMENTAL PROCEDURES

Materials. G-actin was purified from scallops by the method of Spudich et al. (*24*). Fluorescence-labeled F-actin was obtained by stoichiometrically mixing G-actins and rhodamine phalloidin (Molecular Probes No. 4171) in F-buffer [5 mM HEPES (pH 7.2), 0.2 mM ATP, 0.2 mM $CaCl_2$, 100 mM KCl, 2 mM $MgCl_2$] for 24 h at 4 °C. Phalloidin binds to F-actin stoichiometrically and stabilizes it against depolymerization at a decreased critical concentration of actin. p-Lys (Sigma) with defined polymerization degree N and fluorescein isothiocyanate (later denoted as FITC) labeled p-Lys (Sigma) are used as purchased. The p-Lys concentration, C_P, is expressed in terms of Lys monomer unit.

Actin Bundle Preparation. Actin bundles were prepared by mixing F-actin solution (1 μL) with p-Lys solution (9 μL) to yield a 10 μL reaction mixture where actin concentration C_A, expressed in terms of G-actin concentration, was varied from 2.3×10^{-8} to 6.9×10^{-7} M; $C_P(N = 26)$ is 10^{-4} or 2×10^{-4} M; salt (KCl) concentration C_S ranges from 0.01 to 0.25 M. The samples were incubated at room temperature for 60 min except for kinetic experiments and observed by fluorescence microscopy (FM) and transmission electron microscopy (TEM). In the case of kinetic experiments, the reaction mixtures of $C_A = 4.6 \times 10^{-8}$ M, $C_P(N = 26) = 10^{-4}$ M, and $C_S = 0.1$ M were allowed to equilibrate for 5, 10, 20, and 40 min, respectively, and then observed by FM and TEM.

Transmission Electron Microscopy (TEM). TEM observation was performed using a JEOL (JEM-1200EX) at 120 kV acceleration voltage. After incubation of mixtures of F-actin, p-Lys, and KCl at room temperature for 60 min, 10 μL of the sample was dropped on carbon-coated grids (Nisshin EM Co., Tokyo, Japan). After 3 min, 2% uranyl acetate was added to the sample, and the grid was air-dried. The average thickness of the actin bundle D was obtained over 20 samples.

Fluorescence Microscopy (FM). A cover glass was placed on a slide glass equipped with two spacers 1.1−1.4 mm high at both sides to form a cell. A solution of the reaction mixture (about 10 μL) was introduced into the cell by a micropipet. Then the cell was placed on the stage of a fluorescence microscope (Olympus BX 50) and observed under a 60× objective lens. The fluorescence images were recorded by a CCD camera (Olympus CD-300T-RC), and the longitudinal length of actin bundles was measured by using a computer-analyzing program (MetaMorph, Nippon ROPER). The length of actin bundles L was the average over 100 samples. Dual color images of FITC-labeled p-Lys and rhodamine-labeled F-actin were taken by laser scanning confocal microscopy (FV 200, Olympus). After addition of FITC-p-Lys (10^{-6} M) to the F-actin solution and incubation for 60 min, the dual color imaging of actin bundles was performed.

RESULTS AND DISCUSSION

Two Stages of Actin Bundle Formation. Native F-actins are polydisperse in length between 1 and 10 μm, get about 5 μm as average, and begin to grow, forming bundles above a critical p-Lys concentration (C_P^c). The time profiles of the longitudinal (L) and the lateral (D) growth of actin bundles are investigated by fluorescence imaging and TEM imaging, respectively, in the condition of $C_A = 4.6 \times 10^{-8}$ M, $C_P(N = 26) = 10^{-4}$ M, and $C_S = 0.1$ M. L hardly grows before 5 min but afterward begins to grow, and the growth continues until 40 min (Figure 1). In contrast, D growth is nearly completed within 5 min and hardly progresses later on. This result shows that D is determined at the first stage while L is determined at the second stage.

Next, we examine the effect of actin concentration C_A on bundle growth at a constant $C_P(N = 26) = 10^{-4}$ M and $C_S = 0.01$ M. As shown in Figure 2, L increases from 6.7 to 20.0 μm with the increase of C_A from 2.3×10^{-8} to 6.9×10^{-7} M, but D hardly changes despite the considerable

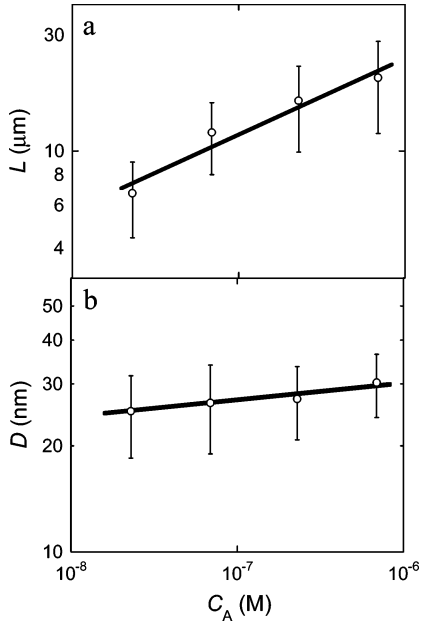

FIGURE 2: Effect of actin concentration C_A on L growth (a) and D growth (b) in $C_P(N = 26) = 10^{-4}$ M and $C_S = 0.01$ M.

increase of C_A. This result indicates that D and L of actin bundles are determined by different factors.

Our results imply that the actin bundle growth consists of two stages. Here, we investigate in detail what induces the anisotropic growth of actin bundles and what determines D and L.

Effect of Binding Energy on Bundle Thickness. As clarified in our previous results, F-actins begin to form bundles cooperatively above C_P^c (*9*, *10*). This C_P^c should be related to energy gain of the self-assembly reaction. That is, the larger the energy gain, the lower the C_P^c.

The electrostatic attraction between the negatively charged F-actin and the positively charged p-Lys should increase with an increase in the degree of polymerization N of p-Lys at a constant ionic strength due to entropy effect. Therefore, we expect an inverse dependence of C_P^c on N. Figure 3 shows the bundle formation of F-actins with p-Lys of various N. As shown in Figure 3a, the critical p-Lys concentration to induce the bundle formation C_P^c decreases dramatically with the increase of N of p-Lys; C_P^c of $N = 3$, 5, 26, and 186 are 7.5×10^{-3}, 5.0×10^{-5}, 5.0×10^{-6}, and 5.0×10^{-7} M, respectively, where C_P^c is expressed in terms of lysine repeated unit. This confirms that the increase in N of p-Lys increases the p-Lys-mediated attraction between F-actins and therefore increases the energy gain by forming a bundle. The charge-fluctuation model also showed that the attraction between F-actins depends strongly on cation valence (*25*). The effect of counterion valence on binding energy can explain why there is a minimum counterion valence required for polyelectrolyte bundle formation: +2 for F-actin bundling and +3 for DNA condensation (*2*, *12*).

From TEM images (Figure 3c), the thickness D of actin bundles formed just above C_P^c decreases with the increase in N, showing values of 59.2 ± 18.2, 41.6 ± 12.7, 33.5 ± 9.4, and 28.4 ± 5.5 nm for $N = 3$, 5, 26, and 186, respectively (Figure 3b). This result reveals that the stronger the attraction between F-actins mediated by polycations, the thinner the bundles formed.

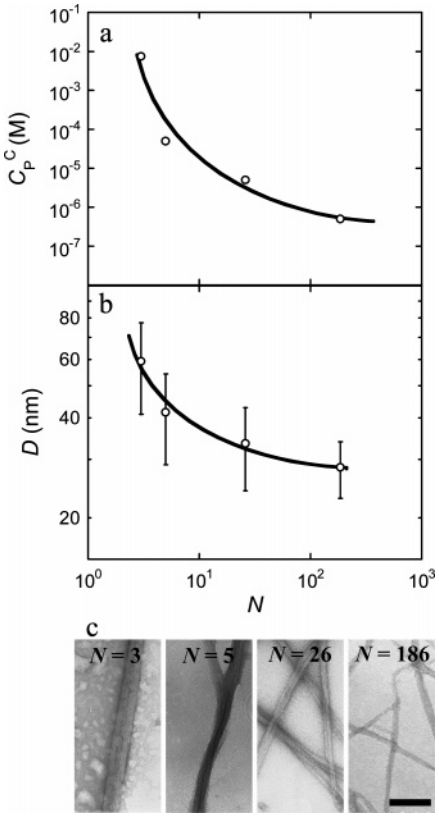

FIGURE 3: Effect of the degree of polymerization N of p-Lys on the actin bundle formation. (a) Dependence of C_P^c on N of p-Lys. (b) Relationship between N and actin bundle thickness D formed just above the critical concentration for bundle formation C_P^c. (c) TEM images of the actin bundle formed just above the C_P^c. $C_A = 2.3 \times 10^{-7}$ M and $C_S = 0.01$ M. Scale bars represent 200 nm.

To confirm the inverse relationship between the attraction energy and the D, we further investigate the effect of ionic strength on D because an elevated ionic strength will screen the condensation of polycation to F-actin and hinder the polycation-mediated attraction between F-actins. We found that in a constant $C_P(N = 26)$ of 2×10^{-4} M, actin bundles are formed in KCl concentration, C_S, ranging from 0.01 to 0.2 M, but no bundles are formed at a higher salt concentration (above 0.25 M). This result shows that salts effectively screen the electrostatic attraction between F-actin and polycation and hinder the polycation-mediated attraction between F-actins.

As shown in Figure 4, D increases from 27.2 to 49.3 nm with the increase of C_S from 0.01 to 0.2 M. This again shows that D increases with the decrease of attraction between F-actins, consistent with the result observed for the effect of N on D in Figure 3. Results in Figures 3 and 4 indicate that D growth cannot be simply understood by the general thermodynamic equilibrium which predicts that an increase in binding energy promotes the growth. A similar phenomenon was reported for the DNA toroids formed in hexamine cobalt solution where the diameter and the thickness of toroids increase with decreasing binding energy by increasing the ionic strength or the temperature (*16*, *17*). This suggests that the inverse relationship between binding energy and intrinsic size of the assembly, that is, the thickness of actin bundles or the size of DNA toroids, results from a common mechanism.

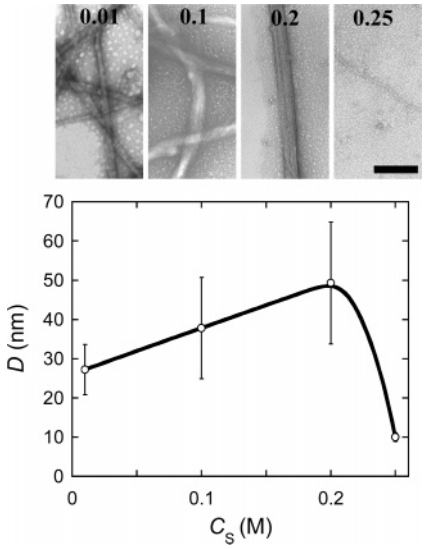

FIGURE 4: Effect of salt concentration C_S on actin bundle formation. TEM images and average thickness of actin bundles formed in various C_S. The numbers on the top of the TEM images are salt concentration, C_S (M). $C_A = 2.3 \times 10^{-7}$ M and $C_P(N = 6) = 2 \times 10^{-4}$ M. Scale bars represent 200 nm.

Anisotropic Nucleation-Growth Mechanism for Actin Bundle Formation. The above experimental results can be summarized as follows:

(1) D is completed at the initial stage of bundle growth, and L dramatically increases later on, after the D growth.

(2) D is weakly dependent on C_A, while L increases with increase in C_A at a constant C_P.

(3) D decreases remarkably with an increase in polycation-mediated attraction between F-actins.

Results 1 and 2 indicate that the self-assembly consists of two stages, and D and L are determined by different factors, respectively; results 2 and 3 indicate that D growth cannot be explained by general thermodynamics. From these results, we conclude that the first stage of actin bundle formation is the nucleation process and the second stage is the growth process. D is determined in the nucleation process by the critical nucleus size D_0, where the stronger the attraction between F-actins, the smaller the critical nuclei that are able to survive. L is determined by the free F-actins available to grow relative to the concentration of stable nuclei. The nucleus concentration is dominated by C_P. As shown in Figure 2, at a constant C_P, D does not change but L increases with the increase of C_A since the concentration of free F-actins relative to nucleus concentration increases and consequently allows each nucleus to grow to a longer size.

Here, we discuss the factor to determine D in more detail. In F-actin and polycation mixing solution, polycations either condensed on F-actins or in the free state are coexistent. Like-charged F-actins are assembled into bundles when the amount of polycations condensed on them increases to a critical value. The free energy, ΔG, of forming bundles can be expressed as $\Delta G = \Delta G_{bulk} + \Delta G_{surf} = -\Delta gV + \gamma S$, where Δg is the energy gain due to bundle formaton of F-actins per unit volume, V is the volume of actin bundles, γ is the surface energy per unit area, and S is the surface area of actin bundles. For the nucleation-growth process, spontaneous growth occurs only when stable nuclei are formed, which occurs when the favorable volume term ΔG_{bulk} surpasses the unfavorable surface term ΔG_{surf}. We regard the bundle as a cylindrical object with a length L and a thickness D. The free energy $\Delta G(D,L)$ for the formation of the bundle is

$$\Delta G = -\frac{\pi D^2 L}{4}\Delta g + \frac{\pi D^2 + 2\pi DL}{2}\gamma \approx -\frac{\pi}{4}(\Delta g D^2 L - 4\gamma DL) \quad (1)$$

where it is assumed that (i) for a newborn nucleus, $D \ll \gamma/\Delta g \ll L$. The behavior of $\Delta G(L,D)$ can be made clear by considering the following two simple paths for change of the arguments: When D remains at a small value and only L increases, the free energy is given by $-(\pi/4)(\Delta g D^2 - 4\gamma D)L$ (the prefactor of L is positive under assumption i). Thus, ΔG monotonically increases along the path; on the other hand, when L remains at a small value and only D increases, the free energy is $-(\pi/4)[(\Delta g L)D^2 - (4\gamma L)D]$, and we have the critical thickness D_0 above which ΔG decreases with increasing D (and also L). This observation tells us that D growth must come ahead to form the stable nuclei. D_0 is determined by the free energy barrier ΔG^* where ΔG is maximum. From $\partial \Delta G/\partial D = 0$, we have

$$D_0 \approx 2\gamma/\Delta g \quad (2)$$

$$\Delta G^* \approx \pi\gamma^2 L/\Delta g \quad (3)$$

Equations 2 and 3 indicate that D_0 and ΔG^* are reciprocally proportional to the energy gain per unit volume for bundle formation Δg. In other words, the increase in polycation-mediated attraction between F-actins decreases D_0, which explains well why D decreases with the increase in binding energy between F-actins under assumption that (ii) the observed thickness D_{ob} of the bundles is slightly larger but very close to D_0.

The remaining problem is how we justify crucial assumption ii. Once nuclei of critical thickness D_0 are formed, growth in D and L both favors the free energy; that is, the growth process is favorable thermodynamically. However, the electrostatic repulsion of side-to-side bundling of F-actins is much stronger than that of end-to-end annealing of F-actins because F-actin is a rodlike polyelectrolyte. Therefore, D growth will be suppressed kinetically but L growth favored kinetically in the subsequent growth process. Accordingly, D should be slightly larger but almost equal to D_0. This explains why F-actin bundles grow in two stages, switching from D growth in the initial stage to L growth later on.

Observation of Nucleation Site. The above discussion shows that D growth is essential for the formation of stable nuclei despite the high electrostatic repulsion of side-to-side bundling of F-actins. Therefore, the nucleation process requires a higher condensation of polycations on F-actins to overcome the high energy barrier due to the strong repulsion between F-actins in side-to-site bundling, in comparison with the end-to-end growth. This suggests that the polycation condensed at the nucleus sites should have a higher density than that of other sites in the bundles. Thus, we examine the polycation distribution in actin bundles by using a FITC-labeled p-Lys. Figure 5 shows that FITC-p-Lyses are not homogeneously distributed but concentrated at some sites in most of the actin bundles. We found that most of the p-Lys concentrated sites in actin bundles have 1−3 μm length.

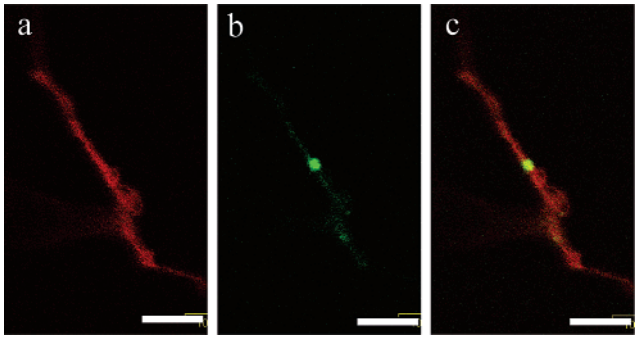

FIGURE 5: Confocal images of the actin bundle by dual imaging of rhodamine phalloidin-labeled F-actin (a), FITC-labeled p-Lys (b), and merge (c). $C_A = 2.3 \times 10^{-7}$ M, $C_P(N = 6) = 10^{-6}$ M, and $C_S = 0.2$ M. Scale bars represent 10 μm.

These p-Lys concentrated sites may be the nuclei to initiate the formation of actin bundles. A possible explanation for why nucleation sites are shorter than average F-actin length is that the shorter F-actins among polydisperse F-actins in length are more favorable for nucleation formation due to the weaker electrostatic repulsion of side-to-side bundling.

CONCLUSIONS

The self-assembly of well-defined actin bundles by interacting with p-Lys is explained in terms of the anisotropic nucleation-growth mechanism, in which the thickness D and the length L of actin bundles are dominated by the critical nucleus size D_0 and the concentration of free actins relative to the concentration of the nucleus, respectively. This mechanism originates from the rodlike polyelectrolyte nature of the F-actins.

This anisotropic nucleation-growth mechanism may be generally applied to the organization of rodlike polyelectrolytes and provides new insight into understanding physical origins of biopolymer self-organization in cells. For example, it was reported recently that the phosphorylation of Ena/VASP induces the reorganization of actins from network (lamellipodia) to parallel bundle (filopodia) (*26*, *27*). However, it has not been understood why phosphorylation can induce their reorganization. Since the dominant interaction between Ena/VASP and actin is electrostatic (*5*), we consider that phosphorylation of Ena/VASP weakens the electrostatic attraction between Ena/VASP and actin and thus decreases the binding energy between actins. According to the reciprocal relationship between the energy gain by bundling and the bundle thickness shown in eq 1, phosphorylation may rather promote the bundling process. Actually, in vitro experiments showed that the phosphorylated VASP induces the formation of thicker bundles than wild-type VASP despite the decrease in the attraction with actins (*6*), which is in agreement with the anisotropic nucleation-growth mechanism.

The anisotropic nucleation-growth mechanism shows that the thickest and most robust bundles are formed near the unstable state, and they can be dramatically disassembled into native F-actins by a slight increase in salt concentration near KCl, 0.2 M (Figure 4). This dramatic transition in structure due to a little change of binding energy might be responsible for the dynamic assembly/disassembly of actins that is biologically essential for cell locomotion, adhesion, and cytokinesis. It remains to be investigated experimentally whether the biopolymer organization based on this model actually occurs in living systems.

ACKNOWLEDGMENT

We are grateful to Mr. Noriaki Ito for advice and assistance on the observation of the TEM images.

REFERENCES

1. Howard, J. (2001) *Mechanics of motor proteins and the cytoskeleton*, pp 110−116, Sinauer, Sunderland, MA.
2. Tang, J. X., and Janmey, P. A. (1996) The polyelectrolyte nature of F-actin and the mechanism of actin bundle formation, *J. Biol. Chem. 271*, 8556−8563.
3. Tang, J. X., Ito, T., Tao, T., Traub, P., and Janmey, P. A. (1997) Opposite effects of electrostatics and steric exclusion on bundle formation by F-actin and other filamentous polyelectrolytes, *Biochemistry 36*, 12600−12607.
4. Needleman, D. J., Ojeda-Lopez, M. A., Raviv, Uri., Miller, H. P., Wilson, L., and Safinya, C. R. (2005) Higher-order assembly of microtubules by counterions: From hexagonal bundles to living necklaces, *Proc. Natl. Acad. Sci. U.S.A. 101*, 16099−16103.
5. Huttelmaier, S., Harbeck, B., Steffens, N. O., Meberschmidt, T., Illenberger, S., and Jockusch, B. M. (1999) Characterization of the actin binding properties of the vasodilator-stimulated phosphoprotein VASP, *FEBS Lett. 451*, 68−74.
6. Harbeck, B., Huttelmaier, S., Schluter, K., Jockusch, B. M., and Illenberger, S. (2000) Phosphorylation of the vasodilator-stimulated phosphoprotein regulates its interaction with actin, *J. Biol. Chem. 275*, 30817−30825.
7. Tang, J. X., Szymanski, P., Janmey, P. A., and Tao, T. (1997) Electrostatic effects of smooth muscle calponin on actin assembly, *Eur. J. Biochem. 247*, 432−440.
8. Amann, K. J., Renley, B. A., and Ervasti, J. M. (1998) A cluster of basic repeats in the dystrophin Rod domain binds F-actin through an electrostatic interaction, *J. Biol. Chem. 273*, 28419−28423.
9. Goldmann, W. H., Guttenberg, Z., Tang, J. X., Kroy, K., Isenberg, G., and Ezzell, R. M. (1998) Analysis of the F-actin binding fragments of vinculin using stopped-flow and dynamic light-scattering measurements, *Eur. J. Biochem. 254*, 413−419.
10. Earnshaw, W. C., King, J., Harrison, S. C., and Eiserling, F. A. (1978) The structural organization of DNA packaged within the heads of T4 wild-type, isometric and giant bacteriophages, *Cell 14*, 559−568.
11. Rao, V. B., and Black, L. W. (1985) DNA packaging of bacteriophage T4 proheads *in vitro* evidence that prohead expansion is not coupled to DNA packaging, *J. Mol. Biol. 185*, 565−578.
12. Bloomfield, V. A. (1991) Condensation of DNA by multivalent cations: considerations on mechanism, *Biopolymers 31*, 1471−1481.
13. Ha, B. Y., and Liu, A. J. (1999) Kinetics of bundle growth in condensation, *Europhys. Lett. 46*, 624−630.
14. Ha, B. Y., and Liu, A. J. (1998) Effect of non-pairwise-additive interactions on bundles of rodlike polyelectrolytes, *Phys. Rev. Lett. 81*, 1011−1014.
15. Yoshikawa, K., Yoshikawa, K., and Kanbe, T. (1999) Formation of a giant toroid from long duplex DNA, *Langmuir 15*, 4085−4088.
16. Conwell, C. C., Vilfan, I. D., and Hud, N. V. (2003) Controlling the size of nanoscale toroidal DNA condensates with static curvature and ionic strength, *Proc. Natl. Acad. Sci. U.S.A. 100*, 9296−9301.
17. Conwell, C. C., and Hud, N. V. (2004) Evidence that both kinetic and thermodynamic factors govern DNA toroid dimension: effect of magnesium(II) on DNA condensation by hexamine cobalt(III), *Biochemistry 43*, 5380−5387.
18. Hud, N. V., Downing, K. H., and Balhorn, R. (1995) A constant radius of curvature model for the organization of DNA in toroidal condensates, *Proc. Natl. Acad. Sci. U.S.A. 92*, 3581−3285.
19. Grosberg, A. Y., and Zhestkov, A. V. (1985) Toroidal globular state of DNA: persistent macromolecule in a low-molecular solvent, *Biofizika 30*, 698−699.

20. Kakugo, A., Shikinaka, K., Matsumoto, K., Gong, J. P., and Osada, Y. (2003) Growth of large polymer-actin complexes, *Bioconjugate Chem. 14*, 1185−1190.
21. Kwon, H. J., Kakugo, A., Shikinaka, Furukawa, K., Osada, Y., and Gong, J. P. (2005) Morphology of actin assemblies in response to polycation and salts, *Biomacromolecules 6*, 3005−3009.
22. Bartles, J. R. (2000) Parallel actin bundles and their multiple actin-bundling proteins, *Curr. Opin. Cell Biol. 12*, 72−78.
23. Alberts, B., et al. (2002) *Molecular biology of the cell*, 4th ed., pp 929−948, Garland Science, New York.
24. Spudich, J. A., and Watt, S. (1971) Regulation of skeletal muscle contraction. I. Biochemical studies of the interaction of the tropomyosin-troponin complex with actin and the proteolytic fragments of myosin, *J. Biol. Chem. 246*, 4866−4871.
25. Radeva, T. (2001) *Physical chemistry of polyelectrolyte*, pp 163−180, Marcel Dekker, New York.
26. Svitkina, T. M., Bulanova, E. A., Chaga, O. Y., Vignjevic, D. M., Kojima, S., Vasiliev, J. M., and Borisy, G. G. (2003) Mechanism of filopodia initiation by reorganization of a dendritic network, *J. Cell Biol. 160*, 409−421.
27. Lebrand, C., Dent, E. W., Strasser, G. A., Lanier, L. M., Krause, M., Svitkina, T. M., Borisy, G. G., and Gertler, F. B. (2004) Critical role of Ena/VASP proteins for filopodia formation in neurons and in function downstream of netrin-1, *Neuron 42*, 37−49.

BI060721W